Raman Spectroscopy of Three Average-Valence Dicopper Cryptates: Evidence for Copper−Copper Bonding

Ala Al-Obaidi,[†] Goran Baranovič,[‡] Joanne Coyle,[†,§] Colin G. Coates,[†] John J. McGarvey,*[,†] Vickie McKee,*[,†] and Jane Nelson*[,†,§]

School of Chemistry, Queens University, Belfast, BT9 5AG U.K., Institut R. Boškovič, 11001 Zagreb, Croatia, and Chemistry Department, Open University, Milton Keynes, MK7 6AA U.K.

Received October 10, 1997

Comparison of the X-ray structures of two pairs of dicopper(I) and dicopper(1.5) cryptates provides evidence (over 0.5 Å contraction of the internuclear distance in one pair) for copper−copper bond formation. Although resonance Raman spectroscopy fails to identify a pure copper−copper stretching mode, because of extensive mixing of several low-frequency stretching and bending modes, isotopic substitution experiments indicate significant Cu−Cu character in a band around 250 cm^{-1}. A normal coordinate analysis broadly supports the spectroscopic findings. X-ray crystal structures are presented for the dicopper(1.5) complex Cu_2*imBT*$(ClO_4)_3$, $C_{18}H_{30}Cl_3Cu_2N_8O_{12}$, $a = 9.140(4)$ Å, $c = 30.35(3)$ Å, rhombohedral, *R*32, $Z = 3$, and the dicopper(I) Cu_2*imbistrpn*$(ClO_4)_2$, $C_{24}H_{42}Cl_2Cu_2N_8O_8$, $a = 9.279(2)$ Å, $c = 32.846(9)$ Å, rhombohedral, *R*32, $Z = 3$.

Introduction

The "blue copper" electron-transfer site was one of the earliest examples of the application of spectroscopic methods[1] to coordination site determination in metalloproteins. Consequently, much was known about the coordination environment of the metal in advance of the solution of any type 1 copper protein crystal structure. X-ray crystallographic[2] confirmation of the spectroscopically deduced donor set and geometry in plastocyanin and azurin established the validity of the spectroscopic approach as a preliminary strategy in metalloprotein structure determination. In these blue copper electron-transfer proteins, the well-conserved distorted tetrahedral N_2SS^- coordination site lies intermediate between the coordination preferences of Cu(I) and Cu(II). The advantages of utilization of "soft" sp^2 N or S donors and of the particular geometric disposition adopted have been analyzed[3] in terms of minimization of potential energy change in the course of electron transfer from the +1 to the +2 redox state of copper. This mononuclear blue copper site is thus well-adapted to its role as an electron-transfer agent, and until recently there was no hint of the existence of copper electron-transfer agents of higher nuclearity than 1, even when the significance of other di- and tricopper bio sites[4] had been recognized. Over the past few years, however, spectroscopic evidence for the existence of dicopper electron-transfer sites has been steadily mounting. In some multielectron redox enzymes, such as nitrous oxide reductase[5] and cytochrome *c* oxidase,[6] the electron-transfer sites could be inferred, on spectroscopic grounds, to contain not one but a pair of copper ions in an average-valence $Cu_2(1.5)$ redox state. The recent structure determination[7] of two forms of cytochrome *c* oxidase confirms these spectroscopic inferences, showing a Cu−Cu separation of 2.5−2.6 Å supported by a dithiolate bridge. The remaining donors—thioether-S, histidine-N, and (in weak long coordination) a carboxylate-O^-—have all been implicated in type 1 copper proteins, so the donor set is not far from typical blue copper ligation, acceptable to both +1 and +2 redox states, but closer to the preferences of Cu(I). The coordination geometry, if the close contact to the second copper is ignored, is also typical blue copper geometry: distorted tetrahedral/distorted trigonal pyramidal, intermediate between +1 and +2 redox state preferences, again relatively favoring Cu(I). The reason for utilization of a dinuclear assembly for the purposes of electron transfer in these redox enzymes is now the topic of lively debate. The significance of the argument over the existence of copper−copper bonding in such average-valent electron-transfer sites tends to be inflated by the recognition that, if this can be demonstrated, it will be the first metal−metal bond in biology. Such metal−metal bonding is not found in the analogous, though spin-localized, Fe_2S_2 electron-transfer site, or in mixed-valence catalytic centers which show localized valence.[8,9]

[†] Queens University.
[‡] Institut R. Boškovič.
[§] Open University.

(1) Gray, H. B.; Solomon, E. I. In *Copper Proteins*; Spiro, T., Ed.; Wiley: New York, 1981; Vol. 3, 1.39.
(2) (a) Guss, J. M.; Freeman, H. C. *J. Mol. Biol.* **1983**, *169*, 526. (b) Norris, G. E.; Andersen, B. F.; Baker, E. N. *J. Am. Chem. Soc.* **1986**, *108*, 2784.
(3) Kaim, W.; Rall, J. *Angew. Chem., Int. Ed. Engl.* **1996**, *35*, 43.
(4) Messerschmidt, A.; Luecke, H.; Huber, R. *J. Am. Chem. Soc.* **1990**, *112*, 9548. Magnus, K. A.; Ton-That, H.; Carpenter, J. E. *Chem. Rev.* **1994**, *94*, 727.
(5) (a) Kroneck, P. M. H.; Antholine, W. E.; Kastrau, D.H.; Buse, B.; Steffens, G. C. M.; Zumft, W. G. *FEBS Lett.* **1990**, *268*, 274. (b) Buse, B.; Zumft, W. G.; Kroneck, P. M. H. *Eur. J. Biochem.* **1992**, *209*, 875.
(6) Farrar, J. A.; Lappalainen, P.; Zumft, W.G.; Saraste, M.; Thomson, A. J. *Eur. J. Biochem.* **1995**, *33*, 10401.
(7) (a) Tsukihara, T.; Aoyama, H.; Yamashita, E.; Tomizaki, T.; Yamoguchi, H.; Shinzawa-Itoh, K.; Nakashima, R.; Yaono, R.; Yoshikawa S. *Science* **1995**, *269*, 1069. (b) Iwata, S.; Ostermeier, C. O.; Ludwig, B.; Michel, H. *Nature* **1995**, *376*, 660. (c) Wilmanns, M.; Lappalainen, P.; Kelly, M.; Saureriksson, E.; Saraste, M. *Proc. Natl. Acad. Sci. U.S.A.* **1995**, *92*, 11955.
(8) Wieghardt, K. *Angew. Chem., Int. Ed. Engl.* **1989**, *28*, 1153.

S0020-1669(97)01274-3 CCC: $15.00
Published on Web 06/20/1998

Although examples of Mn−Mn and Fe−Fe bonding are to be found in organometallic chemistry,[10] Cu−Cu bonding is rare in any chemistry. Thirty years ago or so,[11] there was some discussion of the possible existence of a copper−copper bond in copper(II) acetate, on the grounds that the short (2.6 Å) internuclear separation enforced by the 1,3-carboxylate bridge would ensure overlap of magnetic orbitals in a weak δ bond. However, unambiguous evidence for copper−copper bonding in a synthetic complex was obtained only recently, in a mixed-valence azacryptate,[12] Cu_2*imBT*$(ClO_4)_3$ (**1**). Overlap of d_{z^2} orbitals from the pair of copper ions held in trigonal bipyramidal geometry and in close proximity by the steric constraints of the azacryptand host enforces a one-electron copper−copper σ bond, as demonstrated by both ESR[13] and electronic absorption[14] spectroscopy. Since then, two similar examples[14,15] of mixed-valence dicopper(1.5) cryptates have been synthesized; all three show markedly similar spectral characteristics. In ESR, for example,[13] a seven-line fluid solution ESR spectrum is common to all three dicopper cryptates, as is a seven-line $A_\perp$ hyperfine pattern in the glass spectrum ($A_\parallel$ being too small to be resolved). The seven-line $A_\perp$ pattern is retained down to 4 K which is an unprecedently low temperature for electron delocalization in mixed-valence dicopper, necessitating the designation *average* valence. The hyperfine coupling $A_\perp$ is relatively large (compared with normal Cu^{2+} or, indeed, the Cu_A site of cytochrome *c* oxidase), signifying, in contrast to the blue copper systems, the absence of extensive delocalization of spin density[13] onto the host.

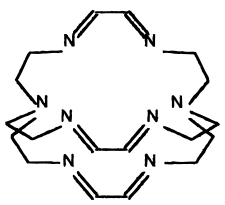

imBT

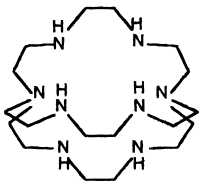

amBT

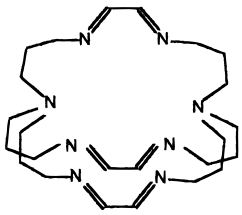

imbistrpn

Despite the difference in unsaturation of the host skeleton, electronic absorption spectra are very similar in the three cases, suggesting, at least for the visible and near-IR absorption, an origin in transitions between molecular orbital levels derived from combination of copper valence orbitals. (In the ultraviolet, intense $\pi-\pi^*$ absorption, expected around 300 nm for hexaimines **1** and **3**, Cu_2*imbistrpn*$(ClO_4)_3$, must account for at least part of the observed absorption below 330 nm; magnetic circular dichroism (MCD) activity is associated with the higher frequency UV band around 285 nm. The more intense UV absorption observed for the octaamine cryptate **2**, Cu_2*amBT*$(ClO_4)_3$, lies in a region associated with LMCT absorption in analogous copper(II) amine chelates.[16]) The high intensity of the far-red/near-IR absorption in all three cryptates confirms that none of the major features is restricted by the selection rules applying to simple d−d transitions. These features, which derive from transitions between molecular orbitals of approximate σ, π, and δ symmetry[17] formed by overlap of pairs of d_{z^2}; d_{xz},d_{yz}; and $d_{x^2-y^2}$, d_{xy} orbitals, respectively, having different "allowedness" and varying degrees of bonding character in their ground and excited states, have recently been assigned[18] on the basis of group theoretical considerations, confirmed by simulation of the associated MCD spectra.

Comparison with the natural dicopper electron-transfer sites was initially hampered by interference from catalytic sites in the intact enzyme. The ESR spectrum of the Cu_A site in nitrous oxide reductase, when separated from other ESR-active signals in the natural enzyme, presents strong evidence for delocalization of the unpaired electron over both copper nuclei. However, in intact cyctochrome c oxidase, heme absorption prevents the observation of ESR or, indeed, electronic spectral features arising from Cu_A other than the broad 830-nm absorption. Cloning of the Cu_A site of *Bacillus subtilis*[19] and *Paracoccus denitrificans*[20] allowed examination of a clean Cu_A electronic absorption spectrum, uncomplicated by overlapping heme bands. A range of water-soluble proteins containing only a single Cu_A center is now available as a result of genetic manipulation, and these reveal common features in both absorption and MCD spectra, which have been assigned,[21] following theoretical simulation based on INDO/S calculations and group theoretical analysis. The "intervalence transition" or one-electron excitation from the symmetric to the antisymmetric orbital $\psi-\psi^*$ combination is assigned at 9000 cm^{-1}, in comparison to 13 000−14 000 cm^{-1} in our average-valent models. However, an alternative assignment, presented in ref 22, prefers the 13 000 cm^{-1} absorption on the basis of enhancement of Cu−Cu modes in the resonance Raman[23] upon 13 000-cm^{-1} excitation.

Resonance Raman studies can be a useful way of investigating the nature of orbitals involved in particular electronic transitions, as the oscillator excited by that transition will be the one whose bonding character is most affected by it. A comprehensive analysis of the resonance Raman spectroscopy of Cu_A has been

(9) Lippard, S. J. *Angew Chem., Int Ed Eng.* **1988**, *27*, 344.
(10) Cotton, F. A.; Wilkinson, G. *Advanced Inorganic Chemistry*, 5th ed.; John Wiley and Sons: New York, 1988; Chapter 23.
(11) Edmonson B. J.; Lever, A. B. P. *Inorg Chem.* **1965**, *4*, 1608 and references therein.
(12) Harding, C. J.; McKee, V.; Nelson, J. *J. Am. Chem. Soc.* **1991**, *113*, 9684.
(13) Harding, C. J.; Nelson, J.; Wyatt, J.; Symons, M. C. R. *J. Chem. Soc., Chem. Commun.* **1991**, 2499.
(14) Farrar, J. A.; McKee, V.; Al-Obaidi, A. H. R.; McGarvey, J. J.; Nelson J.; Thomson, A. J. *Inorg Chem.* **1995**, *34*, 1302.
(15) Barr, M. E.; Smith, P. H.; Antholine, W. E.; Spencer, B. *J. Chem. Soc., Chem. Commun.* **1993**, 1649.
(16) Lever, A. B. P. *Electronic Absorption Spectroscopy*, 2nd ed.; Elsevier: New York, 1984; p 355.
(17) Although not strictly applicable to the symmetries under consideration, these labels are used for reasons of familiarity and convenience.
(18) Farrar, J. A.; Grinter, R.; Neese, F.; Kroneck, P. M. H.; Nelson, J.; Thomson, A. J. *J. Chem. Soc., Dalton Trans.* **1997**, 4083.
(19) van Wachenfeldt, C.; de Vries, S.; van der Oost, J. *FEBS Lett.* **1994**, *340*, 109.
(20) Lappalainen, P.; Aasa, R.; Malstrom, B. G.; Saraste, M. *J. Biol. Chem.* **1993**, *268*, 26416.
(21) Farrar, J. A.; Neese, F.; Lappalainen, P.; Kroneck, P. M. H.; Saraste, M.; Zumft, W. G.; Thomson, A. J. *J. Am. Chem. Soc.* **1996**, *118*, 11501.
(22) Williams, K. R.; Gamelin, D. R.; LaCroix, L. B.; Honser, R. P.; Tolman, W. B.; Mulder, T. C.; Vries, S.; Hedman, B.; Hodgson, K. O.; Solomon, E. I. *J. Am. Chem. Soc.* **1997**, *119*, 613.
(23) Wallace-Williams, S. E.; James, C. A.; deVries, S.; Saraste, M.; Lappalainen, P.; van der Oost, J.; Fabian, M.; Palmer, G.; Woodruff, W. H. *J. Am. Chem. Soc.* **1996**, *118*, 3896.

recently presented by Sanders-Loehr and co-workers.[24] We have previously reported preliminary resonance Raman studies[14,25] on the average-valence dicopper systems **1**−**3**, concentrating on excitation into far-red absorptions. In particular, we found enhancement of a pair of modes below 300 cm^{-1} to depend markedly on the excitation wavelength. In this account, we report the work in fuller detail, extend the wavelength range of the study, and describe the results of ^{65}Cu isotopic substitution experiments. In addition, a normal coordinate analysis of a model system has been carried out in an attempt to elucidate the nature of the low-frequency modes. We are also able to report new X-ray crystallographic studies on dicopper(I) and dicopper(1.5) cryptates, which, after comparison with existing structural data, constitute independent structural evidence for the existence of copper−copper bonding in the average-valence cryptates.

Experimental Section

Spectroscopy. Resonance Raman spectra were recorded over the range 700−950 nm using a Ti-sapphire laser (Spectra Physics model 3900) pumped by an Ar^+ laser (Spectra Physics model 2025). Spectra were recorded in a backscattering geometry on a cooled CCD detector (Princeton Instruments model LN/UV 1152) coupled to a single spectrograph (Jobin-Yvon HR640), with a 300 grooves/mm grating for the near-IR studies or a 1200 grooves/mm element for the UV region. Notch or supernotch holographic filters were used to attenuate laser (Rayleigh) scattering. To enhance detector sensitivity in the red, the CCD was operated at −80 °C instead of the usual −120 °C for the UV−visible region. Saturated aqueous (∼10 mM) solutions of the complexes were used with $NaNO_3$ as internal standard for the construction of excitation profiles.

Normal Coordinate Analysis. The normal cordinate analysis employed the programs of Schachtschneider and Mortimer,[26] modified by inclusion of the damped least-squares method described by Sundius.[27]

Syntheses. Cu_2*imBT*$(ClO_4)_2$ (4) and Cu_2*imbistrpn*$(ClO_4)_2$ (5). These cryptates are most conveniently made by template synthesis on Cu(I), as follows: To a deoxygenated solution of glyoxal (0.3 mmol) in ethanol/acetonitrile (5:1, 30 mL) is added 0.2 mmol of $Cu(MeCN)_4(ClO_4)$. The mixture is brought to reflux, and a solution of the appropriate triamine (0.2 mmol in 5 mL of deoxygenated EtOH) is added under nitrogen. After 10−15-min reflux, the solution is cooled in ice and volume reduced under nitrogen until the yellow/tan crystalline product is obtained.

Analysis. [Cu_2*imBT*]$(ClO_4)_2$ (**4**), found (calculated): N, 16.2 (16.4); C, 31.8 (31.6); H:, 4.3 (4.4); yield 75%. [Cu_2*imbistrpn*]$(ClO_4)_2\cdot 2H_2O$ (**5**), found (calculated): N, 13.8 (13.9); C, 35.6 (35.8); H, 5.3 (5.7); yield 16%. The solid product is aerobically stable, but solutions in EtOH/MeCN can be oxidized to the analogous blue/green mixed-valence cryptates [Cu_2*imBT*]$(ClO_4)_3\cdot 2H_2O$ (**1**) and [Cu_2*imbistrpn*]$(ClO_4)_3\cdot 4H_2O$ (**3**) on treatment[14] with stoichiometric amounts of Ag^+, followed by filtration of the silver metal formed.

Cu_2*amBT*$(ClO_4)_2\cdot 3H_2O$ (2). This cryptate can be made by direct reaction of the free cryptand made as described elsewhere,[28] with 2 equiv of copper(II) perchlorate: To 0.1 mmol of *amBT* in 10 mL of EtOH is added 0.2 mmol of $Cu(ClO_4)_2\cdot 6H_2O$ in 10 mL of MeCN. A bright blue color is immediately observed, and the intensely blue microcrystalline product is isolated on standing in air to reduce volume.

Table 1. Crystallographic Data for Cu_2*imBT*$(ClO_4)_3$ (**1**) and Cu_2*imbistrpn*$(ClO_4)_2$ (**5**)

	1	**5**
chemical formula	$C_{18}H_{30}Cl_3Cu_2N_8O_{12}$	$C_{24}H_{42}Cl_2Cu_2N_8O_8$
formula weight	789.93	768.64
T (°C)	−120(2)	−120(2)
λ (Å)	0.71073	0.71073
space group	*R*32 (No.155)	*R*32 (No.155)
a (Å)	9.140(4)	9.279(2)
c (Å)	30.35(3)	32.846(9)
V (Å$^{3)}$	2196(2)	2449(1)
Z	3	3
ρ_{calcd} (g/cm^3)	1.779	1.563
μ (mm^{-1})	1.799	1.523
R1 [$I > 2\sigma(I)$][a]	0.0994	0.0755
wR2 (all data)[b]	0.2464	0.2274

[a] $R1 = \sum||F_o| - |F_c||/\sum|F_o|$. [b] $wR2 = [\sum[w(F_o^2 - F_c^2)^2]/\sum[w(F_o^2)^2]]^{1/2}$.

Analysis. Cu_2*amBT*$(ClO_4)_2\cdot 3H_2O$ (**2**), found (calculated): N, 13.2 (13.2); C, 25.4 (25.2); H, 5.1 (4.9); yield 70%.

Cu*imBT*$(ClO_4)_2\cdot H_2O$ (6). This mononuclear cryptate can also be best obtained by direct reaction of the free cryptand made as described elsewhere[28] with the copper(II) salt. To 0.1 mmol of *imBT* in 2:1 $CHCl_3$/EtOH (5 mL) is added 0.1 mmol of $Cu(ClO_4)_2\cdot 6H_2O$ in 5 mL of EtOH, and the brown microcrystalline product is filtered off on standing.

Analysis. Cu*imBT*$(ClO_4)_2\cdot H_2O$ (**6**), found (calculated): N, 17.3 (17.5); C, 34.1 (33.8); H, 4.7 (5.0); yield 85%.

Safety Note: Perchlorate salts must be treated as potentially explosive.[29] However, we did not experience any problems in the synthesis with the conditions and on the scale described. However, particular care must be exercised when attempting to record Raman spectra, which should, for prudence, be restricted to the solution phase.

X-ray Experimental Data. Crystal data for **1** and **5** are summarized in Table 1. Diffraction data for both crystals were collected at −120 °C on a Siemens P4 four-circle diffractometer using graphite-monochromated Mo Kα radiation. Data sets were corrected for Lorentz and polarization effects, and empirical absorption corrections were applied.[30] Both structures were solved by direct methods[31] and refined by full-matrix least-squares on F^2 in space group *R*32, using all the data. All the non-hydrogen atoms were refined with anisotropic atomic displacement parameters, except for some of those involved in disorder. Hydrogen atoms were inserted at calculated positions, with isotropic displacement parameters riding on U_{ij} of their carrier atoms. There was some disorder at the C1 position in **1**, modeled as equal occupancy of two equivalent sites, and in the perchlorate anions. Structure **5** was refined as a racemic twin (50% of each component). In each case, refinement in the lower symmetry space group *R*3 was attempted but did not remove the disorder or improve the refinement. All programs used in the structure refinement are contained in the SHELXL-93 package.[32]

Results

Resonance Raman (RR) spectra of **1**−**3** have been recorded in the UV at 363.8 nm where possible and over a range of wavelengths spanning the visible−near-IR absorption for all three complexes. The principal features in 363.8 nm spectra appear at frequencies >300 cm^{-1}, with no clearly discernible bands occurring at lower frequencies. RR spectra at this excitation wavelength for **1** and **3** were weak and of insufficient quality to be of use. This is partly the consequence of poor match of the exciting frequency with significant absorption in

(24) Andrew, C. R.; Fraczkiewicz, R.; Czernusewicz, R. S.; Lappalainen, P.; Saraste, M.; Sanders-Loehr, J. *J. Am. Chem. Soc.* **1996**, *118*, 10436.
(25) al-Obaidi, A. H. R.; Qin, L.; Bell, S. E. J.; Nelson, J.; McGarvey, J. J. *Proceedings XIVth ICORS*, Yu, N.-T., Li, X.-Y., Eds.; John Wiley and Sons: New York, 1994; p 252.
(26) Schachtschneider, J. H.; Mortimer, F. S. Technical Reports Nos. 57−65; Shell Development Co.: Emeryville, CA, 1965.
(27) Sundius, T. *J. Mol. Spectrosc.* **1980**, *82*, 138.
(28) Smith, P. H.; Barr, M. E.; Brainard, J. R.; Ford, D. K.; Freiser, H.; Muralidharan, S.; Reilly, D. D.; Ryan, R. R.; Silks, L. A.; Yu, W. H. *J. Org. Chem.* **1993**, *58*, 7939.
(29) See for example: *Chem. Eng. News* **1983**, *61* (Dec.), 4.
(30) Sheldrick, G. M. *SHELXTL*, Version 4; Siemens Analytical X-ray Instruments: Madison, WI, 1990.
(31) Sheldrick, G. M. SHELXS-86. *Acta Crystallogr.* **1990**, *A46*, 467.
(32) Sheldrick, G. M. *SHELXL-93*; Universität Göttingen: Göttingen, Germany, 1993.

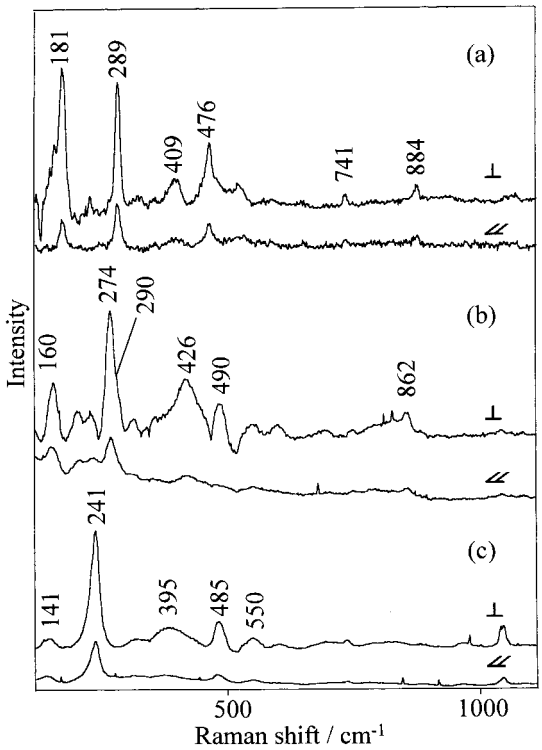

Figure 1. Resonance Raman spectra for complexes **1**−**3** (traces a−c, respectively) in millimolar aqueous solutions. Laser excitation wavelengths: (a) 840, (b,c) 810 nm. Laser power at sample, 25−30 mW.

the hexaimine cryptates but may also derive from differences in the nature of the transition excited at this wavelength in the octaamine versus hexaimine systems.

RR studies over the range 700−910 nm enabled a more detailed study of the vibrational mode patterns as a function of excitation wavelength (λ_{exc}). Figure 1 shows representative spectra for all three complexes. The notable feature of these is the appearance of several polarized bands at frequencies below 300 cm^{-1}, in the ranges 240−290 cm^{-1}, specifically at 289 (**1**), 274, 290 (**2**), and 241 cm^{-1} (**3**) and in the range 140−181 cm^{-1}, at 181 (**1**), 160 (**2**) and 141 cm^{-1} (**3**), together with a number of higher frequency polarized features extending to 1000 cm^{-1} and beyond, attributable to overtone and combination bands. Excitation profiles for the 160- and 274-cm^{-1} features for complex **2** are presented in Figure 2a. The 274-cm^{-1} band is part of a doublet, and the other component, at 290 cm^{-1}, shows a different excitation profile, more closely coincident with the electronic band maximum (Figure 2, inset). The maximum resonance intensity for the 274-cm^{-1} feature lies near 770 nm (around 10−20 nm to long wavelength of the absorption maximum) and that for the 160 cm^{-1} mode toward yet lower energies, >800 nm, suggesting the existence of several contributions to the electronic absorption. The short-term stability of **1** in aqueous solution increased the difficulty of constructing an extensive excitation profile in this instance, but the results of a more limited study are shown in Figure 2b. It is clear also in this case that both modes are enhanced through excitation within the near-IR absorption envelope, although the maximum enhanced intensity does not coincide with the near-IR absorption maximum for either mode. The same pattern is noted in Figure 2c for the third cryptate, **3**, although in this case, where the near-IR maximum lies farthest to the red, the falloff in detector response prevented location of the excitation profile maximum for either of the two modes.

To provide more information on the nature of the low-frequency modes, studies were carried out on isotopically substituted complexes. RR spectra were recorded for ^{65}Cu-substituted samples of **1** and **2**. The results at λ_{exc} = 810 nm are shown in Figure 3. For **1**, the 181-cm^{-1} band shows a small but reproducible shift of ca. 0.7 cm^{-1}. That for the mode at 289 cm^{-1} is significantly larger, 1.7 cm^{-1}. These findings have been confirmed for **1** at two other excitation wavelengths, 710 and 910 nm. In the case of **2**, the 160-cm^{-1} mode again exhibits only a small shift of 0.7 cm^{-1}, but for both the 274- and 290-cm^{-1} modes, the shift is appreciable, 1.7 cm^{-1}. Bearing in mind the errors in peak locations, these results are substantially in agreement with other independent isotope shift data reported by Woodruff and co-workers[33] for the octaamine cryptate **2**.

FTIR spectra recorded for **1** in CsI disks are shown in Figure 4 and, for comparison, spectra of the mono-Cu^{II}*imBT*$(ClO_4)_2$ (**6**) and the di-Cu^{I}*imBT*$(ClO_4)_2$ (**4**) complexes were also measured. A number of bands were observed in the frequency range 180−400 cm^{-1}. Only in the case of the average valence complex were bands observed in the region ca. 250−260 cm^{-1}. However, we were unable to check via isotopic substitution the possibility that these bands might be associated with Cu−Cu motion, as any anticipated isotope shifts would fall within the resolution attainable.

In view of the large number of vibrational degrees of freedom for the three complexes **1**−**3**, coupled with a lack of sufficiently comprehensive vibrational data, an approximate normal coordinate analysis (NCA) only has been attempted. This was performed on the 10-atom skeletal structure, N−CuN_3−CuN_3−N (common to all three cryptates and hereafter referred to as CuN), taken to belong to the point group D_3, inferred from the X-ray structures. We assume that D_3 symmetry applies in solution, even though lower symmetry may exist in the solid state or other matrixes.

The relevant structural parameters for CuN are given in Table 2. The reducible representation for the 10-atom system in the assumed D_3 point group is composed of the vibrational modes, $5A_1 + 3A_2 + 8E$. For convenient reference in subsequent discussion, the internal coordinates used in this work are labeled and described in Table 3. There are 24 of them, i.e., no redundant coordinates are present because the A, B, and Λ coordinates are defined to conform to the local symmetry requirements. Since the charge distributions along the principal C_3 axis are expected to differ substantially from those orthogonal to this axis, distinct force constants are defined to describe the Cu−axial-N and Cu−equatorial-N stretching coordinates. It may be remarked here, in what is admittedly a somewhat crude NCA of these dicopper cryptates, that effective masses for the nitrogens should be used to simulate the effects of neglected atoms on the ligands. However, in view of the necessary interdependence of motion within these interconnected ligand chains, there appears to be no simple way of choosing optimum values for the nitrogen masses. Instead, the following approach was adopted: taking m_N as 14.0067, isotope data for $[^{63}Cu_2amBT]^{3+}$ and $[^{65}Cu_2amBT]^{3+}$ from resonance Raman spectra reported by Woodruff et al.,[33] were used to generate an initial force field for this system. Six of the force constants in Table 3 were adjusted to fit eight frequencies, the remainder being assigned "reasonable" values on the grounds that they exert no influence on the A_1 modes. The force constants that emerge from the initial input data (see ref 33) for the

(33) Shreve, A. P.; Franzen, S.; Wallace-Williams, S. E.; Barr, M. E.; Woodruff, W. H. Poster presentation at XV ICORS, University of Pittsburgh, Pittsburgh, PA, 1996.

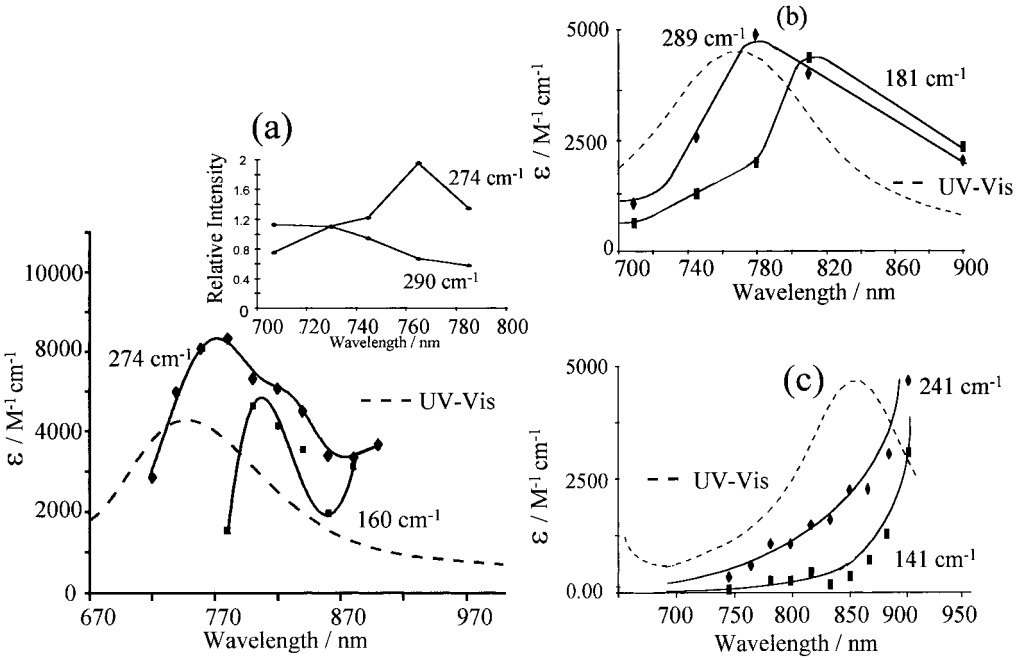

Figure 2. Resonance Raman excitation profiles: (a) For the 160 and 274-cm $^{-1}$ features of complex **2**. Inset: Comparison of the excitation profile of the 274-cm^{-1} feature with that of the 290-cm^{-1} component of the partly resolved doublet in the spectrum. All spectra were recorded in millimolar aqueous solution, with 1050-cm^{-1} band of $NaNO_3$ as internal standard. (b) For the 181- and 289-cm^{-1} features of complex **1**. (c) For the 141- and 241-cm^{-1} bands of complex **3**. Experimental conditions are as in (a).

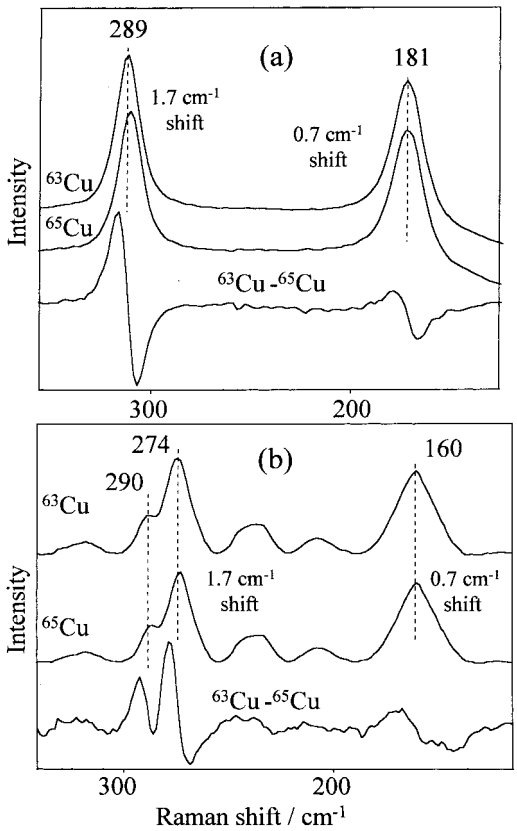

Figure 3. Influence of isotopic substitution (^{63}Cu → ^{65}Cu) on the low-frequency region of the resonance Raman spectra of complexes **1** and **2**, traces a and b, respectively. Spectra of the individual isotopomers and the corresponding difference spectra are shown in each case. Spectra were recorded using 810-nm excitation (30 mW at sample) in saturated aqueous solution.

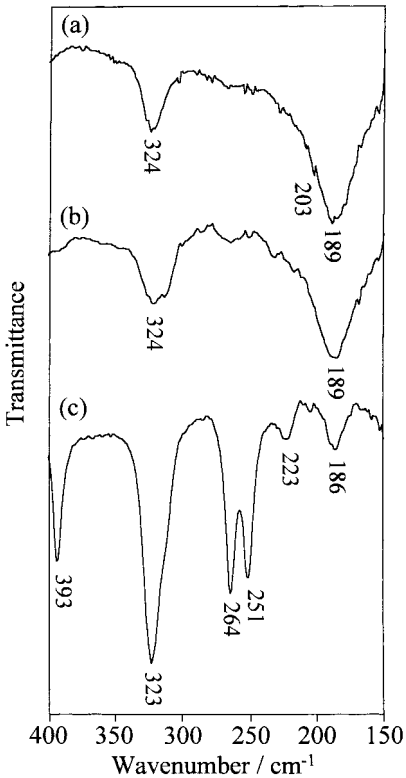

Figure 4. CsI disk IR spectra of $[Cu_2imBT]^{2+}$ (**4**), trace a; $[CuimBT]^{2+}$ (**6**), trace b; and $[Cu_2imBT]^{3+}$ (**1**), trace (c).

$[^{63}Cu_2amBT]^{3+}$ and $[^{65}Cu_2amBT]^{3+}$ complexes are shown in this table. In view of the highly approximate nature of the NCA used here, detailed comment on the magnitudes of the force constants is largely unwarranted. While the magnitudes are smaller than might be expected, we have no baseline values with which to make comparison in the present instance. Values a factor of 2 larger cited for a Cu−N bond by Sanders-Loehr et al.[24] refer to a bond from Cu to an imidazole ring, treated as a single-point mass of 67 and quite different from the situation in the present systems, where the difficulty in selecting optimum values for the nitrogen atom masses has already been referred

Table 2. Structural Parameters (Bonds, Å, and Angles, deg) for Dicopper(I) and Dicopper(1.5) Complexes

parameter	$Cu_2imBT(ClO_4)_2$ (**4**)	$Cu_2imBT(ClO_4)_3$ (**1**)	$Cu_2imbistrpn(ClO_4)_2$ (**5**)	$Cu_2imbistrpn(ClO_4)_3$ (**3**)	$[Cu_2amBT](NO_3)_3$[c]
Cu−Cu	2.448(1)	2.380(5)	2.928(4)	2.419(1)	2.364(1)
Cu−N_{ax}	2.218(3)	2.04(2)	2.22(2)	2.055(1)[a]	2.066(5)[a]
Cu−N_{eq}	1.999(3)	1.96(2)	2.01(1)	2.022(4)[a]	2.067(5)[a]
N_{ax}−Cu−N_{eq}	84.9(1)	85.5(4)	95.2(4)	93.7(1)[a]	86.1(1)[a]
Cu distance from equatorial plane[b]	0.18	0.15	−0.18	−0.13	0.13[a]

[a] Mean of independent values. [b] Positive values describe displacement of the copper ion toward the center of the cage. [c] Data for the nitrate salt (ref 15) rather than the perchlorate (**2**).

Table 3. Force Constants for CuN Obtained from Isotopic Frequency Shifts[a] for $[^{63}Cu_2amBT]$ and $[^{65}Cu_2amBT]^{3+}$

internal coordinate description	coordinate label	force constant[b,c]	error[d]
Cu−N_{ax} stretch	R	0.628	0.023
Cu−Cu stretch	Q	1.558	0.337
Cu−N_{eq} stretch	S	0.873	0.001
symmetry-adapted combination of N_{ax}−CuP−N_{eq} bends	A	1.134	0.098
symmetry-adapted combination of N_{eq}−Cu−N_{eq} bends	B	2.700	0.0
symmetry-adapted combination of N_{ax}−Cu−Cu linear bends	Λ	0.110	0.0
torsional mode	T	2.900	0.0
(Cu−N_{ax} stretch)(Cu−Cu stretch) interaction	RQ	0.178	0.045
(Cu−N_{ax} stretch)(N_{ax}−Cu−N_{eq} bend) interaction	RA = −QA	−0.184	0.109

[a] Reference 33. [b] Other interaction force constants not shown here were given fixed zero values. [c] Force constants in mdyn/Å (stretch), mdyn Å/rad (bend). [d] Zero error means that the corresponding force constant was kept fixed.

Table 4. Observed and Calculated Isotopic Frequency Shifts (cm^{-1}) and Potential Energy Distributions[a] (PED)

	$[^{63}Cu_2amBT]^{3+}$			$[^{65}Cu_2amBT]^{3+}$		
ν_i[b]	obsd	calcd	PED	obsd	calcd	PED
1(A_1)	327.0[c]	327.2	96S	327		97S
2(A_1)	289.0[d]	289.0	90R 55Q 15A	286.6[d]	286.8	101R 41Q 10A
3(A_1)	275.0[d]	275.0	39Q 28A 20R	273.0[d]	273.2	52Q 34A
4(A_1)	164.0[d]	163.8	68A 17Q	163.3[d]	163.6	67A 17Q

[a] See Table 3 for coordinate descriptions. [b] Symmetry species in D_3. [c] See Figure 1. [d] Reference 33.

to. The point is given further consideration below. Although the relative magnitudes of the force constants in Table 3 for the Cu−N_{ax} and Cu−N_{eq} bonds are qualitatively in line with the crystallographic data in Table 2, being somewhat smaller for the longer bonds, not too much significance should be attached to this, either, since the NCA is based on complex **2**, for which the Cu−N_{ax} and Cu−N_{eq} distances differ by only 0.01 Å. The force field derived from **2** was then used to calculate vibrational frequencies for complexes **1** and **3**, with $m_N = 14.0067$ and $m_{Cu} = 63.546$. The results for the lowest frequency modes, <300 cm^{-1}, together with the potential energy distributions (PEDs), are not much different from those for complex **2**, shown in Table 4, because the geometry differences between the CuN models are not large enough. Although the spectral region up to ca. 1100 cm^{-1} has been probed, we concentrate on the region <400 cm^{-1} for the purposes of comparison with the results of the NC analysis. Complete listings of the calculated and observed frequencies for complex **2** are given in Tables S1 and S2 (Supporting Information). Using the spectroscopic data for complex **1**, for which isotopic shifts have been measured for two features (Figure 3), a different force

Table 5. Observed and Calculated Frequencies (cm^{-1}) and Potential Energy Distribution[a] (PED) $(Cu_2imBT)^{3+}$, with Effective Nitrogen Atom Masses $N_{axi} = 14.0067$ and $N_{eq} = 12.0067$

	frequency			PED		
ν_i	obsd	calcd	diff			
1		359.5		98SA_1		
2	289.0	289.1	−0.1	72QA_1	69RA_1	31AA_1
3		281.8	0	40RA_1	25AA_1	14QA_1
4	181.0	181.2	−0.2	55AA_1	25QA_1	
5		469.1		99TA_1		
6		352.5		99SA_2		
7		297.3		104RA_2		
8		246.8		100AA_2		
9		730.5		45BE	26ΛE	
10		636.2		83BE		
11		496.9		53BE	21ΛE	
12		449.6		50ΛE	18AE	
13		378.2		87SE		
14		368.2		87SE		
15		210.1		76AE	12ΛE	
16		167.8		61AE	23ΛE	

[a] See Table 3 for coordinate description.

field was obtained. This is to be expected, since agreement between the force fields from the two sets of spectroscopic data would imply that the effective nitrogen masses are 14.0067 for both ligands *imBT* and *amBT* and, moreover, that 14.0067 represents the effective mass of both the equatorial and axial nitrogens. This seems highly improbable. The point here is that, starting from the above force field based on the data for complex **2**, it would be possible to match the observed data for **1** and **3** simply by introducing $m_{N-axial}$ and $m_{N-equatorial}$ as fitting parameters. For instance, to produce a band at 289 cm^{-1} for **1**, it is sufficient to reduce $m_{N-axial}$ to about 13 and $m_{N-equatorial}$ to about 12. However, this influences not only the frequencies but also the nature of the normal modes (Table 5). Quite analogously, a band at 250 cm^{-1} in the RR spectrum of **3** could also be produced, but with somewhat different values of reduced masses.

Despite the approximate nature of the NCA, a number of interesting conclusions emerge. Most strikingly, the PEDs show that the Cu−Cu stretching vibration is strongly coupled not only to Cu−N_{axial} stretching motion but also to N_{ax}−Cu−N_{eq} bending coordinates. These points are taken up in the Discussion.

$[Cu_2imBT(ClO_4)_3]^{3+}$ (**1**) had earlier proved difficult to crystallize because of its rapid decomposition in organic solvents. While carrying out spectroscopic experiments, we became aware that the average-valent form of this cryptate could be stabilized by using an excess of silver ion, and eventually small, X-ray-quality crystals were isolated from aqueous solutions containing excess Ag^+. Previous structural data on the $[Cu_2imBT]^{3+}$ system were inferred only, from the fact that the mixed-valent form could be successfully doped into dicopper(I) crystals in 30% proportion.[12] The ease with which the dicopper(1.5) form can be doped into the dicopper(I) $imBT(ClO_4)_2$ lattice can be

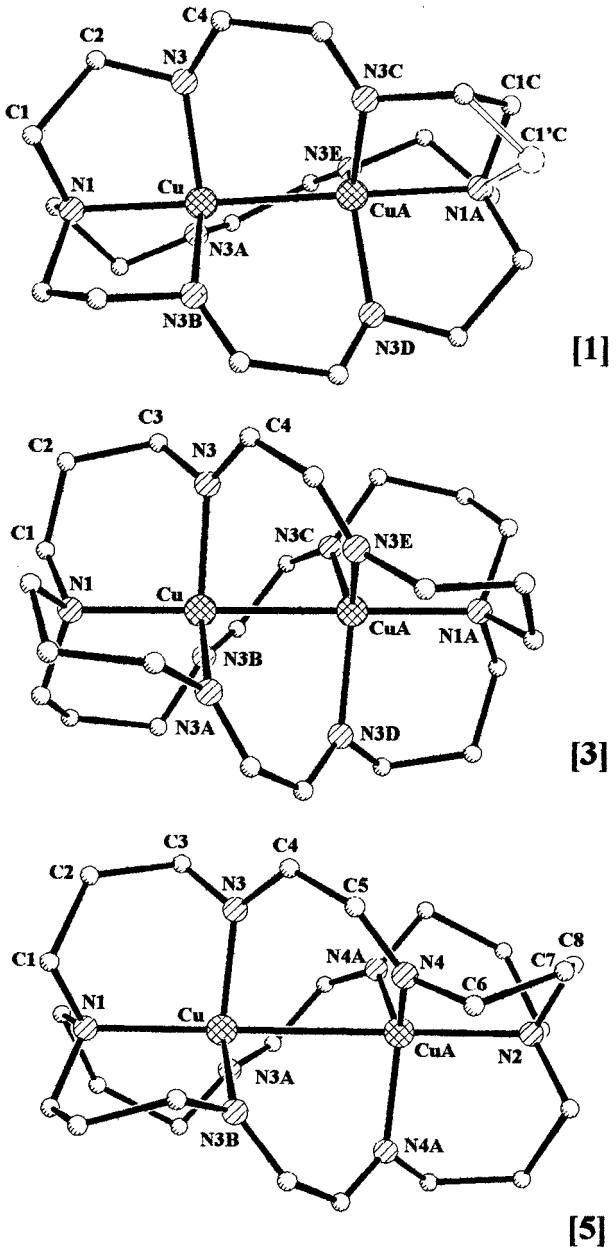

Figure 5. Perspective views of the cations $[Cu_2imBT]^{3+}$ (**1**), $[Cu_2imbistrpn]^{3+}$ (**3**), and $[Cu_2imbistrpn]^{2+}$ (**5**). Hydrogen atoms are omitted, and the disorder in the strands of **1** is shown for only one of the six equivalent sites (C1c and C1c′). The three figures are on the same scale.

explained by comparison of the unit cell packing of the two complexes. The structures differ only in the presence of an extra perchlorate anion on the 3-fold axis in **1**. Indeed, if this is ignored, the lattices of **1**, **4**, and **5** can be superimposed, while that of **3** differs only by a doubling of the *c* axis. Our new X-ray crystallographic structure determination of **1** allows the determination of bond lengths with greater accuracy than before. It makes possible, for example, comparison of the actual copper−copper internuclear distance in both redox states (Figure 5 and Table 2).

Discussion

(i) Structural Evidence. The structures of the cations from dicopper(1.5) $imBT(ClO_4)_3$ (**1**) and dicopper(I) *imbistrpn* $(ClO_4)_2$ (**5**), along with the previously reported structure of the average-valence dicopper(1.5) *imbistrpn* cryptate (**3**), are shown in Figure 5. Relevant bond distances are given in Table 2. Immediately noticeable on comparison of **3** and **5** is the >0.5-Å shortening of the copper−copper internuclear distance from 2.928(4) to 2.419(1) Å on going from the dicopper(I) to the dicopper(1.5) redox state. This change takes place without any other major structural alteration, except for the overall reduction of the $N_{bridgehead}-N_{bridgehead}$ distance and the subsequent tightening of the helical pitch in the methylene link. The slight shortening of the $Cu-N_{bridgehead}$ distance in the mixed-valent versus the dicopper(I) form may reflect some small degree of delocalization of the bond density onto the bridgehead nitrogens, as suggested by ESR results.[13]

In the case of $[Cu_2imBT(ClO_4)_3$ (**1**), steric constraint in the rigid small host does not allow for much relaxation of the copper−copper internuclear distance in the nonbonded dicopper(I) form, and there is limited opportunity to reflect copper−copper bond formation through alteration of internuclear distances. However, a small but significant shortening from 2.448(1) to 2.380(5) Å is discernible, which does support the idea of bond formation in the average-valent form.

(ii) Spectroscopic Evidence. As the principal vibrational bands in the region <800 cm^{-1} in the RR spectra of **1**−**3** are polarized (Figure 1), totally symmetric modes with contributions from Cu−Cu and Cu−N stretching and N−Cu−N bending coordinates are expected. It is clear from the excitation profiles in Figure 2 for the primary features in the 140−185- and 250−295-cm^{-1} ranges, that at least two electronic transitions contribute to the near-IR absorption profile in the range 700−900 nm. This conclusion is consistent with the Gaussian analysis of the MCD and electronic absorption spectra of **1** and the consequent assignment[18] of the electronic spectrum, which indicates the main near-IR band to contain unresolved absorptions lying to low frequency of the maximum. Although we had earlier anticipated, in the absence of isotope data, that modes associated with Cu−Cu motion would most probably lie at frequencies <200 cm^{-1}, the new measurements presented here on isotopically substituted complexes show that the real situation is more involved than this, with substantial mode mixing taking place. Nevertheless, from the magnitude of the shift in the features near 290 cm^{-1} in the spectra (Figure 3) of **1** and **2** upon ^{65}Cu substitution, −1.7 cm^{-1}, compared with the much smaller shift of − 0.7 cm^{-1} in the lower frequency (160, 181 cm^{-1}) bands, it would appear that copper−copper motion is more involved in the *higher* frequency mode. Our results and those of Woodruff and co-workers[33] on complex **2** appear to be in agreement on this point. Also in agreement is the assignment[18] of the electronic spectrum of **1**, which confirms that the most intense feature of the near-IR absorption corresponds to a $\sigma-\sigma^*$ transition. Assignment of the band near 750 nm in the electronic and MCD spectra as arising from the fully allowed $\sigma-\sigma^*$ transition would be expected to give rise to enhancement of the Cu−Cu stretching mode in the RR spectrum upon 750 nm excitation. The isotope data show that the largest contribution from a Cu−Cu stretch is to the 270/290-cm^{-1} feature, and this is in line with the excitation profile. The NCA does not however indicate the existence of a pure Cu−Cu stretching mode, although the 270/290-cm^{-1} mode shows a greater contribution from a Cu−Cu stretching coordinate than does any other (Tables 4 and 5).

Both RR and MCD data indicate additional component(s) in the near-IR envelope. Irradiation at longer wavelengths excites a second, lower frequency mode, which the isotope shifts indicate to have a smaller contribution from Cu−Cu motion. The assignment[18] of the electronic spectrum suggests that this

component is being enhanced upon excitation of a $\delta-\sigma^*$ transition, which may be expected to affect $Cu-N_{eq}$ as well as Cu−Cu orbital overlap. The NCA suggests substantial contribution in this case from the $N_{eq}-Cu-N_{ax}$ bending motion. It is interesting in this connection to note that IR-*active* modes at around 180−190 cm^{-1} are seen in both mono-Cu^{II} and di-Cu^{I} as well as in the average-valence cryptates. We do not know to what extent D_3 symmetry applies within the CsI matrix in which IR spectra were measured; the fact that bands in the region of 250−265 cm^{-1} appeared in the IR, for the average-valence complex alone, might suggest that A_2 normal modes are being observed. In D_3, these are IR-active only, involving contributions from S and R stretching and A bending coordinates (see mode descriptions in Table 3) and are expected in that frequency region according to normal mode calculations (Tables S1 and S2, Supporting Information). It appears, therefore, that the observed vibrational spectra can be explained on a D_3 model.

Although we have ignored any interaction of Cu−Cu and Cu−N vibrational modes with cryptand skeletal modes, such interaction undoubtedly influences the observed frequencies to some extent. The trends in the low-frequency modes, 181 (*imBT*), 160 (*amBT*), and 141 cm^{-1} (*imbistrpn*), are qualitatively in accord with expectation in this respect. Interaction with skeletal modes of the cryptand will be most marked in the tightest and most rigid cryptand (*imBT*) and least marked in the more flexible *imbistrpn*.

Conclusion

Despite the unavoidable mixing of modes in these strongly coupled oscillators, which prevents the observation of a pure Cu−Cu stretching motion, we can conclude that the mode with the greatest share of this motion is a relatively high-frequency one, in the range 270−290 cm^{-1} in all three cases. The force constant emerging from the NCA is unexpectedly high for a one-electron bond, almost double that attributed to Cu−Cu stretching in the Cu_A site of cytochrome *c* oxidase. Although it compares favorably with that of Cu_2, which involves a two-electron bond,[34] not a great deal should be read into this comparison, since two 4s electrons are involved in the latter, rather than three 3d electrons in **1**−**3**. To some extent, the value of the force constant must reflect the neglected coupling of Cu−Cu and Cu−N modes with skeletal modes of the cryptand, but it also emphasizes the efficiency of interaction between appropriately disposed copper d-orbitals in mixed-valence dicopper systems. The striking reduction in Cu−Cu distance in the *imbistrpn* system upon one-electron oxidation from the dicopper(I) state likewise illustrates the facility with which the one-electron bond may be formed.

It is unsurprising that this facile and efficient mode of interaction has been exploited in biochemistry, even though it was until recently undiscovered in chemistry. However, it seems clear from the comparison of bond lengths,[7] force constants,[24] and the recently estimated double-exchange "delocalization factor" [18] that the copper−copper bond in our cryptates is considerably stronger than that in the natural site. There, the weaker Cu−Cu interaction reflects the contribution to bonding in Cu_A of the thiolate bridging, which may play an important functional role in the electron-transfer process.

The chemical applications of the new mode of metal−metal bonding remain to be explored and exploited. One likely application of these novel copper−copper bonded systems is as mild reversible redox reagents. Other applications may follow from their redox-switchable, intense near-IR absorption.

Acknowledgment. We thank EPSRC for support, Grant No. GR/F42980, and a studentship (to J.C.). We are grateful to Drs. W. H. Woodruff and A. P. Shreve for allowing us to use their isotopically shifted frequency data for **2**.

Supporting Information Available: Tables S1 and S2, listing observed and calculated frequencies and potential energy distributions for $[^{63}Cu_2amBT]^{3+}$ and $[^{65}Cu_2amBT]^{3+}$, and Tables S3−S12, listing atomic coordinates, bond lengths and angles, and anisotropic atomic displacement parameters for **1** and **5** (12 pages). X-ray crystallographic files, in CIF format, for the structures are available on the Internet only. Ordering and access information is given on any current masthead page.

IC971274Z

(34) Huber, K. P.; Herzberg, G. *Molecular Spectra and Molecular Structure, Vol. IV, Constants of Diatomic Molecules*; Van Nostrand Reinhold Co.: New York, 1979; p 198. Rohlfing, E. A.; Valentini, J. J. *J. Chem. Phys.* **1986**, *84*, 6560.